EFDA–JET–PR(08)22

V. Yavorskij, V. Kiptily, C. Challis, V. Goloborod'ko, L.G. Eriksson, N. Hawkes, P. Neuruer, S. Reznik, K. Schoepf, S.E. Sharapov, D. Stork, I. Voitsekhovitch, K.-D. Zastrow and JET EFDA contributors

Modelling of γ-Ray Diagnostics for MeV Energy Range Ions in JET

Modelling of γ-Ray Diagnostics for MeV Energy Range Ions in JET

V. Yavorskij[1,2], V. Kiptily[3], C. Challis[3], V. Goloborod'ko[1,2], L.G. Eriksson[4], N. Hawkes[3], P. Neuruer[1], S. Reznik[1,2], K. Schoepf [1], S.E. Sharapov[3], D. Stork[3], I. Voitsekhovitch[3], K.-D. Zastrow and JET EFDA contributors*

JET-EFDA, Culham Science Centre, OX14 3DB, Abingdon, UK

[1]Association EURATOM-OEAW, Institute for Theoretical Physics, University of Innsbruck, Austria
[2]Institute for Nuclear Research, Ukrainian Academy of Sciences, Kiev, Ukraine
[3]EURATOM-UKAEA Fusion Association, Culham Science Centre, OX14 3DB, Abingdon, OXON, UK
[4]Association EURATOM-CEA, CEA/DSM/DRFC, CEA-Cadarache, France
** See annex of M.L. Watkins et al, "Overview of JET Results ",*
(Proc. 21 st IAEA Fusion Energy Conference, Chengdu, China (2006)).

Preprint of Paper to be submitted for publication in
Nuclear Fusion

ABSTRACT.
The paper investigates the temporal evolution of γ-ray emission induced by nuclear interactions between energetic fusion-born alpha particles with beryllium impurity ions in JET plasmas. The alpha slowing down time and loss rates are assessed from the delay time between γ-emission and alpha production in deuteron-triton fusion reactions during tritium NBI blips into a JET deuterium plasma. The use of γ-diagnostics is also demonstrated for examining the energy distributions of ICRH accelerated ^{4}He-ions in the MeV energy range.

1. INTRODUCTION

The investigation of fusion alpha particles produced in JET by short tritium NBI pulses (blips) into deuterium plasmas in Trace Tritium Experiments (TTE) [1,2] and of RF accelerated ^{4}He-ions in Alpha-Particle Simulation Experiments (APSE) [3,4] by the use of γ-diagnostics [5] is a new and promising approach in the study of fast ion behaviour in tokamak plasmas. In these experiments, the information on fast alphas is inferred from measurements of γ-ray emission from nuclear interactions of alphas with beryllium impurity ions (^{9}Be(α,$n\gamma$)^{12}C). One of the most important issues to be addressed to the diagnostics of such γ-rays is the possibility of assessing experimentally the confinement properties of energetic α-particles and of drawing conclusions on their spatial and velocity distributions. This is of particular interest in plasmas with new types of magnetic topology, such as the Current Hole (CH) equilibrium observed in JET [4] and JT-60U [5].

In previous modelling [6-10] it was found that the interpretation of the experimentally observed evolution of α-induced γ-ray emission in TTE requires not only the calculation of α-particle transport, but also an equally accurate description of the time dependence and the shape of the fusion source in phase space. In Ref. [9] the possible evaluation of loss and/or slowing-down rates of fusion alphas from the delay time between production in fusion reactions and induced γ-emission was shown to be a viable technique.

Here we present a detailed modelling of the temporal evolution of the distribution of a-particles produced by tritium NBI blips in JET deuterium plasmas and manifest requirements for reliable evaluation of fast alpha confinement based on γ-diagnostics. Further we analyze the relaxation of the distribution function of RF heated ^{4}He ions due to the drop of ICRH power and demonstrate the possible examination of the energy distributions of ICRH accelerated alphas in JET via g-diagnostics.

The paper is organized in the following way. As a first step, a qualitative 1D Fokker-Planck analysis of evolutions of γ-emission is performed in Sec.2 as induced by specific time-varying α-particle distributions. Then Sec.3 contains the results of experimental observations of time-dependent alpha-induced γ-emission in JET as well as results of corresponding time-dependent 1D and 3D Fokker-Planck modelling. Finally, a summary and the concluding discussion are presented in Sec. 4.

2. EVOLUTION OF γ-EMISSION INDUCED BY TIME-DEPENDENT A-S (1D QUALITATIVE ANALYSIS)

In the case of steady-state beryllium ion density at low temperature, the time evolution of the γ-emission rate R_γ is determined as

$$R_\gamma(t) \propto \int dE E f_a(E, t)\, \sigma_\gamma(E), \tag{1}$$

where σ_γ denotes the $^9\mathrm{Be}(\alpha,n\gamma)^{12}\mathrm{C}$ reaction cross-section substantial only for alpha energies $E \geq E_\mathrm{m}$=1.6 MeV, and for the purpose of a qualitative analysis here, only an energy and time-dependent alpha distribution function, $f_\alpha(E,t)$, is referred to. Accounting for losses by the average loss time (τ_l) - approximation this distribution function is found from the simple kinetic equation

$$\partial_t f = 2E^{-1/2}\, \tau s^{-1}\, \partial_E (E^{3/2} f) - f/\tau_l + S(E, t), \tag{2}$$

where the critical energy of alphas, $E_\mathrm{c}(\cong 37T_e) << E_\mathrm{m}$, is neglected due to the MeV energy range of interest. The RHS of Eq. (1) can be readily expressed as

$$R_\gamma(t) \propto \int_{E_m}^{\infty} dE\sqrt{E} \int_0^{\tau_{\alpha\gamma}} d\tau \sigma_\gamma(E')\, \sqrt{E'}\, exp\left(-\frac{\tau}{\tau_l}\right)\, S(E, t-\tau) \tag{3}$$

with

$$E' = E exp\left(-\frac{2\tau}{\tau_s}\right),\ \tau_{\alpha\gamma} = \frac{\tau_s}{2}\ 1n\ \frac{E}{E_m}, \tag{4}$$

where the Spitzer slowing down time is determined by the electron temperature and density as $\tau_\mathrm{s} \propto T_e^{3/2}/n_e$, S is the alpha source rate and $\tau_{\alpha\gamma}$ is the slowing down time of alphas from their birth energy to the threshold energy E_m.

2.1 SHORT TERM MONOENERGETIC ALPHA SOURCE

In the simplest case of a monoenergetic alpha source effective only in an infinitesimal time interval at t = 0, i.e. $S \propto \delta(E- E_0,t)$, the temporal evolution of the gamma emission rate

$$R_\gamma(t)\, exp\left(-\frac{t}{\tau_1}\right)\, \sigma_\gamma(E)\sqrt{E},\ E = E_0\, exp\left(-\frac{2\tau}{\tau_s}\right) \tag{5}$$

is predominantly determined by alpha losses and the energy dependence of the cross section σ_γ.

This evolution of gamma emission produced by a $\delta(E-E_0,t)$-source with E_0 = 3.5 MeV is displayed in Fig.1. It is seen that in the case of well confined alphas the maximum *g*-ray emission is induced by α's slowed down to energies ~ (1.6÷2) MeV and appears delayed in comparison to the alpha production by about 30% of the Spitzer slowing down time. Alpha loss, e.g. taking $\tau_l < \tau_s/3$, will

essentially reduce the gamma emission as well as its delay as is seen in Fig. 2. As a quantitative characteristic of gamma emission delay we use the time shift $\tau_{d\gamma}$ of the "centroid" of $R_\gamma(t)$ against the alpha source centroid, which is determined by the moment when the gamma yield is half of its total, i.e. . Inspection of Fig. 2 shows that the gamma emission induced by well confined alphas appears delayed by

$$\tau_{d\gamma}\,(no\ loss) =: \tau^0_{d\gamma} \equiv \tau_{d\gamma}\,(\tau_l >> \tau_s) \simeq 0.24\tau_s \simeq 0.6\tau_{ay}, \tag{6}$$

while, as the alpha confinement is degraded corresponding to a loss time $t_l = t_s/3$, the γ- delay is reduced by $0.08t_s$ ($\sim 0.2\tau_{\alpha\gamma}$).

To interpret the γ-emission delay time and to illustrate how it can serve for diagnostic purposes, we comparatively analyse the temporal evolution of the fast alpha population with $E > E_m$, i.e.

$$N_a\,(t, E > E_{min}) = \int_{E_{min}}^{\infty} dE E^{1/2} \int_0^{\tau_{\alpha\gamma}} d\tau\ exp\,(-\tau/\tau_l) S(E, t-\tau)\,. \tag{7}$$

We choose to introduce a 'cumulative life time' of alphas with $E > E_m$ by

$$\tau_\Sigma\,(t) = \int_0^t dt' N_a\,(t', E > E_m). \tag{8}$$

Noting that for $S \propto \delta(E\text{-}E_0, t)$ the fast alpha population is $N_\alpha(t, E{>}E_m) \sim \exp(-\tau/\tau_l) \quad \tau \le \tau_{\alpha\gamma}$, the time behaviour of τ_Σ can be expressed as ∀

$$\tau_\Sigma\,(t) \propto [1 - exp(-t/\tau_l)]\ H\,(\tau_{\alpha\gamma} - t) \tag{9}$$

with the symbol H designating the Heaviside step function. In analogy to the γ-delay time, we use τ_Σ, i.e. the characteristic time of alpha population evolution, to introduce a so-called alpha delay time $\tau_{d\alpha}$ defined as the time shift between the centroid of $N_\alpha(t, E{>}E_m)$ and the centroid of the alpha source by $\tau_\Sigma\,(\tau_{d\alpha}) = 0.5\tau_\Sigma\,(\tau_{\alpha\gamma})$ and explicitly calculated as

$$\tau_{d\alpha} = tl\ 1n\ \frac{2}{1 + exp\,(-\tau_{\alpha\gamma}/\tau_l)} \tag{10}$$

which, for the case of perfect alpha confinement, yields $\tau^0_{d\alpha} \equiv \tau_{d\alpha}(\tau_l >> \tau_s) = 0.5\tau_{\alpha\gamma}$ with the superscript "0" designating here and in the following the case of zero alpha loss. From Eq. (10) it becomes evident that the alpha delay time is, for long slowing down times ($\tau_{\alpha\gamma} > \tau_l$), again strongly effected by the loss time of alphas. The deviation of $\tau_{d\alpha}(\tau_l \neq 0)$ from $\tau^0_{d\alpha} = 0.5\tau_{\alpha\gamma}$ is displayed in Fig.3, where for the alpha loss case $\tau_l = \tau_s/3$ the time shift of the centroid of the number of alphas is $\tau_{d\alpha}(\tau_l = \tau_s/3) \approx 0.36\tau_{\alpha\gamma}$ and hence close to the centroid shift of gamma emission, $\tau_{d\gamma}\,(\tau_l = \tau_s/3) \approx 0.39\tau_{\alpha\gamma}$ (Fig.1). Thus, here in the case of most pronounced time dependence of the alpha source, the evolution

of alpha population corresponds well with the evolution of alpha induced g-emission and hence gamma diagnostics with adequate temporal resolution can reasonably characterise the behaviour of MeV alphas.

2.2 EFFECT OF THE SOURCE'S TEMPORAL PROFILE ON THE EVOLUTION OF FAST ALPHAS

First we consider well confined alphas ($\tau_l >> \tau_s$) and the simplest case of a step-like time dependence of a monoenergetic source, i.e. $S(E,t) \propto \delta(E\text{-}E_0)$ $s(t) = \delta(E\text{-}E_0)\mathrm{H}[t(\Delta t\text{ -}t)]$ with Dt designating the duration of alpha production. This kind of source, illustrated in Fig. 4 by the shadowed area, facilitates straight-forward integration of Eq. (7) and supposing monoenergetic S_t yields $N_\alpha(t) \sim G(\Delta t + \tau_{\alpha\gamma}\text{-}t) + G(-t) - G(\Delta t - t) - G(\tau_{\alpha\gamma} - t)$, with $G(x) \equiv xH(x)$ and $\tau_{\alpha\gamma} = \tau_{\alpha\gamma}(E_0)$. Typical shapes of $N_\alpha(t)$ are shown in Fig.4a as depending on the ratio of $\Delta t/\tau_{\alpha\gamma}$. In the case of long periods of fusion alpha production, $\Delta t > \tau_{\alpha\gamma}$, the maximum of N_α occurs when the source is active, whereas for short term alpha sources ($\Delta t \leq \tau_{\alpha\gamma}$) the alpha density reaches its maximum only at shut-down of $S(t)$ and remains for $\tau_{\alpha\gamma} - \Delta t$. Obviously, this difference is caused by the dissimilarity of the distribution functions $f_\alpha(E, t = \Delta t)$ at the moment of source "shut-down" ($t = \Delta t$) as displayed in Fig.4b. For sufficiently long periods of alpha production, $\Delta t > \tau_{\alpha\gamma}$, the energy distribution of slowing down alphas for $E > E_\mathrm{m}$ approach the steady-state solution $f_s(E)$ that would be formed by a stationary source. Due to $\tau_{\alpha\gamma} < \Delta t$ the alpha distribution is given sufficient time for complete relaxation to E_m. Of interest to g-diagnostics is the population of alphas exceeding E_m at any time considered. For that we examine the time dependence of $N_\alpha(E \geq E_\mathrm{m}, t)$ for *short* and *long* term alpha production. In Fig.4 it is seen that in the case of $\Delta t > \tau_{\alpha\gamma}$ the decay of $N_\alpha(E \geq E_\mathrm{m})$ due to deceleration to $E < E_\mathrm{m}$ begins with the source break-down and is characterised by the decay time τ_N for the decrease of $N_\alpha(E \geq E_\mathrm{m})$ from maximum to zero, which for well confined alphas approaches $\tau_{\alpha\gamma}$. Differently, in the case of short alpha source periods, $\Delta\tau < \tau_{\alpha\gamma}$, the production time is too short for complete relaxation of fusion alphas during Δt. The relaxation to E_m happens after source break-down and takes the time $\tau_{\alpha\gamma} - \Delta t$. Since for that the fast alpha distribution is, due to continuous slowing down, steadily shifted towards lower energies, the alpha density decays – after relaxation to E_m – during a time interval equal to the source duration Δt. Because such distinct temporal behaviour can be expected to be reflected also in alpha induced γ-emission, the measurement of decay times of γ-emission [1] will allow for conclusion on alpha slowing down rates in the case of long-time fusion sources. Note that for short-term sources the decay times are determined by the source duration Δt and hence do not tell about MeV-alpha kinetics. Nevertheless, the delay of γ-emission against the fusion alpha source provides the required information about fast alpha behaviour, even in the case of short term alpha production. To demonstrate this we use the delay of fast alpha population compared to their source S, generally given by $\tau_{\delta\alpha} = t_N - t_S$, where t_S denotes the moment when the yield of fusion-born alphas is half of the total alpha yield over the time interval Δt, and similarly t_N designates the moment when the 'cumulative life time' of alphas, i.e. the time integral of N_α, reaches

one half of its total value, i.e.

$$\int_0^{t_X} dtX\,(t) = 0.5 \int_0^{\Delta t + \tau_{\alpha\gamma}} dtX\,(t),\ X = S, N. \qquad (11)$$

Taking here, in the case of a step-like source, $t_S = \Delta t/2$ and $t_N = (\tau_{\alpha\gamma} + \Delta t)/2$ we obtain the simple delay time $\tau_{\delta\alpha} = \tau_{\alpha\gamma}/2$, if alpha losses can be neglected. It is independent of the fusion source duration (see Fig.4) and coincides with delay time $\tau^0_{\delta\alpha}$ (Eq.10) of well confined fast alphas produced by $S \propto \delta(E\text{-}E_0,t)$.

In the next step let us consider JET TTE-like temporal shapes of the fusion alpha source generated by tritium ions injected into a deuterium plasma (Pulse No: 61348, injection period $t_{blip} = 0.1$s) and examine the evolution of fast alpha population and of g-emission. Figure 5 demonstrates the enhancement of both the delay of alpha build up and the delay of γ-emission when the slowing-down time increases. One might expect a noticeable discrepancy in the evolution of gamma-emission and of MeV alpha population due to the essential energy dependence of the cross-section σ_γ. However, direct calculations demonstrate only a weak dissimilarity of the time behaviour $R_\gamma(t)$ and $N_\alpha(E>E_m,t)$ for typical TTE conditions. However, the effect of $\sigma_\gamma(E)$ becomes important in the case of relatively large $\tau_{\alpha\gamma} > 200$ms (corresponding to Spitzer slowing down times $\tau_s > 600$ms). Though the discrepancy of the temporal shapes of R_γ and N_α is significant for large $\boldsymbol{\tau}_{\alpha\gamma}$, the dissimilarity between their delay times remains small.

This is confirmed by Fig.6 displaying the delay times of fast alpha population and gamma emission as a function of slowing down time $\boldsymbol{\tau}_{\alpha\gamma}$. It is seen that for the TTE-like $s(t)$-shape considered the difference between $\tau_{d\alpha}$ and $\tau_{d\gamma}$ is rather small (<10%) for $\tau_{\alpha\gamma}$<0.5s and depends only slightly on the energy spectrum of the fusion source (Fig.6b). In the case of large slowing-down rates ($\boldsymbol{\tau}_{\alpha\gamma}$<0.1-0.15s) both delay times are close to $0.5\boldsymbol{\tau}_{\alpha\gamma}$~$0.19\boldsymbol{\tau}_s$, while weaker deceleration ($\boldsymbol{\tau}_{\alpha\gamma}$>0.2s) yields $\tau_{d\alpha} \approx \tau_{d\gamma} \cong 0.6\boldsymbol{\tau}_{\alpha\gamma}$~$0.23\boldsymbol{\tau}_s$. These estimations settle the time scale of the delay of γ-emission in JET TTE plasmas around 20% of the Spitzer slowing down time. In spite of the wide energy spectrum of the alpha source because of substantial beam-target and beam-beam fusions, and regardless of the essential time spread of the fusion source in the post-blip period the delay of alpha induced γ-emission can be well detected, particularly in the case of large slowing down times and short blips. This is confirmed by Fig.7 displaying the modelled evolution of α-induced γ-emission as a function of alpha energy for a typical tritium NBI blip plasma in JET. As evident there, the maximum γ-ray emissivity is induced by alphas slowed down to energies ~ 1.9 MeV. The time of peak emission is seen to be delayed against the maximum fusion source strength $s(t)$ at the end of the T blip by about 100 ms, which is about $0.15\tau_s$. Note that the time shift between these maxima is small compared to the 250 ms integration time of g-signals in TTE. Therefore an accurate evaluation tool has to be suggested to detect delay times and, which seems to be the shift of centroids of γ-emission yield and of fusion alpha yield (equivalently determined with neutron diagnostics).

2.3 EFFECT OF ALPHA LOSS

As expected, a considerable effect of alpha loss is observable on the time behaviour of alpha population build up. Fig.8 demonstrates the evolution of the normalized fast alpha population as altered by enhancement of losses. High loss rates corresponding to a loss time $\tau_l \leq \boldsymbol{\tau}_{\alpha\gamma}$ are seen to substantially reduce the delay of alpha population with respect to fusion source. As evident from Fig.9, plasmas with a higher Spitzer slowing down time ($\propto T_e^{3/2}/n_e$) and, consequently, higher $\tau_{\alpha\gamma}$ allow for investigation of a wider range of alpha loss rates via delay time measurements. Conveniently, in this wider range the dependence of the delay time $\boldsymbol{\tau}_{d\alpha}$ on τ_l is most pronounced. In contrast, if $\tau_l > \boldsymbol{\tau}_{\alpha\gamma}$ the loss induced reduction of delay time is in the order of only 10-15% and may be useless for diagnostics in view of the time resolution of γ-signals.

2.4 RELAXATION OF STEADY-STATE MAXWELLIAN-LIKE ALPHA DISTRIBUTIONS

Source driven steady state distributions of fast ions can be of several kinds depending on the source. In the specific case of RF heating of injected ^{4}He ions [3, 4], a Maxwellian-like distribution $f \propto \exp(-E/T_f)$ with an effective temperature $T_f > 0.5\ MeV$ may be realised [14]. For ideal confinement such a steady state Maxwellian can e.g. be formed by a model source of fast ions such as

$$S_m(E) = -2E^{-1/2}\tau_s^{-1}\partial_E\,[(E^{3/2} + E_c^{3/2})f_m(E)],\ f_m(E) = f_0\ exp\ (-E/T_f), \tag{12}$$

effective during a time $\Delta t > \boldsymbol{\tau}_s$ and where f_m denotes the Maxwellian distribution with the factor f_0 independent of E,t. Examining the build up of well confined Maxwellian alphas during RF and their relaxation after RF switch-off can be described by Eq.(2) using the alpha source

$$S_\alpha(E, t) = S_m(E)\ H\,[-t(\Delta t + t)]. \tag{13}$$

Introducing this source, which is turned off at $t = 0$, into Eq. (7) and supposing $\boldsymbol{\tau}_s$ = const we arrive at the following expression for the relaxing population of well confined fast alphas

$$N_\alpha^0(t \geq 0, E > Em)\ f_0 \int_{E_1}^{\infty} dE E^{1/2}\ exp\ (-E/T_f),\ E_1^{3/2} = (E^{3/2}{}_m = (E_c^{3/2} + E^{3/2})\ exp\ [3t/\tau_s] - E_c^{3/2}, \tag{14}$$

which can be rewritten in the compact form

$$N_\alpha^0(t) = N_\alpha^0(0)\ \frac{F[E_1(t)/T_f]}{F[E_m/T_f]}\ ,\ F(z) = \sqrt{z}\ exp(-z) + \frac{\sqrt{\pi}}{2}\ erfc(\sqrt{z}), \tag{15}$$

where $erfc(z) = 1 - erf(z)$ and $erf(z)$ is the error function. Recall that the superscript "0" stands for the case of ideal alpha confinement ($\tau_l = \infty$). Generalization to the case of alpha loss results in the following expression

$$N_\alpha(t; \tau_l) = exp\ (-t/\tau_l)\ N_\alpha^0(t). \tag{16}$$

Typical evolutions of the population $N_\alpha(t \geq 0, E > E_m)$ of well-confined alphas after RF shut down, which are of interest in view of interpreting the time behaviour of alpha induced g-signals, are shown in Fig.10 depending on the effective temperature T_f. The decay of well confined alphas with Maxwellian distributions around T_f ~ 1-2 MeV occurs on a time scale in the order of the Spitzer slowing-down time and evidently speeds up with lower effective temperature. Of course, also alpha losses will reduce the decay time, especially when $\tau_l << \tau_s$. These conclusions can be drawn as well from the analysis of the decay time of alpha population defined by $1/\tau_N = -d\ln N_\alpha/dt$. Using Eq. (16) we can express this decay time as

$$\tau_N = \tau_N^0 \tau_l / (\tau_N^0 + \tau_l) , \tag{17}$$

where τ_N^0 represents the decay time of N_α in the case of ideal confinement. Explicit expressions for $N_\alpha(t)$ given by Eq. (15) allow for the compact asymptotic approximation of

$$\tau_N^0 \cong \tau_N^{00} exp(-t/\tau_*) \tag{18}$$

with

$$\tau_N^{00} \cong \tau_s \frac{T_f}{E_m}\left(0.585 + 0.0876 \frac{T_f}{E_m}\right), \quad \tau_* \cong \tau_s \left(1.22 + 0.21 \frac{T_f}{E_m}\right). \tag{19}$$

This expression for τ_N^0 illustrates a nearly linear increase of the decay time of N_α with effective temperature and Spitzer slowing-down time. Further it indicates the decrease of τ_N^0 with time and, consequently, the relaxation of alpha population happens faster than by exponential decay. Equation (15) describes the full relaxation of the population of E>1.6MeV alphas from the steady-state level $N_{\alpha max}$ to the final level $N_{\alpha min} = 0$ in the absence of the fast alpha particle source (when RF power is switched-off). However, in APSE the ICRH power applied for ^{4}He ions acceleration was only partly (about 40%) reduced in the ICRH notches from maximum to a non-zero minimum value. For a realistic description of accelerated ^{4}He ions in APSE we modify our analysis and suppose that at the reduced level of ICRH power, P_{ICRH}^{min}, their distribution function after relaxation is a steady-state Maxwellian with the effective temperature $T_{f\min} = T_{f\max} P_{ICRH}^{min} / P_{ICRH}^{max}$ [14] and with the finite steady-state level of the population of E>1.6MeV alphas $N_{\alpha min} \neq 0$. Accounting for the non-zero source term at t>0 corresponding to minimum ICRH power for the population of E>1.6MeV alphas we obtain the following expression

$$N_\alpha^0(t) = N_{\alpha\, max} \frac{F[E_1(t)/T_{fM}]}{F[E_m/T_{fM}]} + N_{\alpha\, min}\left(1 - \frac{F[E_1(t)/T_{fM}]}{F[E_m/T_{fM}]}\right) \tag{20}$$

describing the partial relaxation of N_α from $N_{\alpha max}$ (possessing a steady-state energy distribution established at maximum P_{ICRH}) to $N_{\alpha min} \neq 0$ (forming a steady-state energy distribution at reduced

P_{ICRH}). The contribution of the non-zero source to $N_a(t)$ at t>0, given by the second term on the RHS of Eq. (20), is demonstrated in Fig. 11. Finally, Fig. 12 displays the resultant temporal evolution of the population of fast ($E>E_m$) Maxwellian-like alphas depending on the value of the effective temperature in the case when $N_{\alpha min}/N_{\alpha max}$ = 0.4. Comparing the time dependences of $N_\alpha(t)$ in Fig.12 and Fig.10 we conclude that finite values of $N_{\alpha min}/N_{\alpha max}$ reduce the decay rates of fast alpha population in comparison to those corresponding to full relaxation ($N_{\alpha min}$=0) but do not influence the sensitivity of N_α decay rates to the effective temperature of alphas. What we comprehend by this 1D kinetic qualitative analysis is that g-diagnostics may serve to evaluate the effective temperature of RF heated ions as well as their confinement.

3. EXPERIMENTAL OBSERVATIONS OF TIME-DEPENDENT ALPHA-INDUCED γ-EMISSION IN JET

We analyze here the time-dependent g-emission induced both by fusion alphas in TTE experiments and by ^{4}He ions accelerated via third harmonic Ion-Cyclotron-Resonance Heating (ICRH) in a-particle simulation experiments on JET. Figure 13 displays the γ-detectors line-of-sight (LoS) in the toroidal (a) and poloidal cross-section (b) of JET. Further shown in this figure are the trajectories of on-axis and off-axis co-injected neutral beams of tritium in TTE and, respectively, of ^{4}He in APSE.

Interpretive modelling of fusion alpha induced g-emission in TTE was carried out based on a 3D time-dependent Fokker-Planck code that accounts for only first orbit (FO) loss of fast alphas and neglects their diffusive transport.

3.1 DELAY OF ALPHA-INDUCED γ-EMISSION IN TTE: EXPERIMENTAL EVIDENCES AND MODELING RESULTS

Our qualitative analysis indicated that preferable discharges for observing gamma delays are those with longer slowing-down times and shorter NBI blip duration. Moreover, such discharges are advantageous for assessing possible alpha loss effects, as only strong losses with $\tau_l < \tau_{\alpha\gamma} \cong 0.4\tau_s$ significantly reduce the γ-emission delay. Table 1, in which q_0 denotes the safety factor in the plasma center, summarizes the basic parameters of 6 shortest-blip TTE discharges on JET with different qualities of alpha confinement, which are subjects of the analysis here.

Shot No	*I/B*, MA/T	τ_{s0}, *ms*	q_0	τ_{blip}, *ms*	*FO loss, %*	$\tau_{d\gamma}$*(exp), ms*	$\tau_{d\gamma}$*(mod), ms*
61131	2.3/2	280	<1	150	~19	<26	18
61151	1.4/1.65	420	>1	100	~44.5	3-53	102
61158	2/2.45	440	>1	150	~17	45-106	93
61346	2.5/3.2	620	>>1	100	17-19	40-127	121
61347	2.5/3.2	640	>>1	100	17-19	58-121	135
61348	2.5/3.2	690	>>1	100	18-19	49-128	125

Table 1: Basic parameters and delay times for 5×250ms time interval

In this context we consider Current Hole (CH) plasmas (Pulse No's: 61346, 61347, 61348) and Monotonic Current (MC) plasmas (Pulse No's: 61131, 61151, 61158). The safety factor profiles are represented for MC plasmas in Fig.14 and, respectively, for CH discharges in Fig.15. We note that a significant sawtooth activity was observed during tritium NBI in Pulse No: 61131. Hereto Fig.16 demonstrates nearly a 1 keV drop in electron temperature and about 30% reduction of the DT neutron emission in the plasma core as caused by sawtooth activity towards the end of blip. Figure 17 displays the time behaviour of γ-ray intensity, R_γ, measured in the CH plasma of Pulse No: 61348 (I_p/B_t = 2.5MA/3.2T) with a 0.1s blip duration and a Spitzer slowing down time in the core of t_{s0} = 0.69s. The delay of γ-emission becomes apparent from Fig.18, where the measured $R_\gamma(t)$ is, due to the delay, still higher than the DT neutron emission rate averaged over the time interval corresponding to the integration time of the γ-measurements (= 250ms). Here the delay time, measured as the shift between the centroids of γ-ray and neutron emission in the time interval of 5×250ms, is 89ms. Figure 19 compares the measured $R_\gamma(t)$ in two CH discharges with nearly identical plasma parameters (I_p/B_t = 2.5MA/3.2T, τ_{s0}=0.62-0.64s) but different temporal behaviour of the fusion rate as indicated by the measured neutron emission rates N14. The alpha slowing down in both discharges was quite similar as evident from Fig.20. Also the g-delay times of both discharges are very close ($\tau_{d\gamma} \approx$ 0.08-0.09s) disregarding the essential difference of the temporal source shapes and of $R_g(t)$, because both the g-emission rates as well as the fusion rates differ in a corresponding way. Thus this indicates the relevance of $\tau_{d\gamma}$ as a characteristic for alpha slowing down and confinement.

For MC plasma discharges Fig.21 compares the measured delays of R_γ with those following from the 3D Fokker-Planck model [3, 6] , which result in overestimated delay times due to neglecting alpha losses other than FO loss.

Expectedly, Figures18 and 21a,b demonstrate this overrating of γ-emission by the FP model applied here. For the CH plasma of Pulse No: 61348 (dotted curve) the measured γ-emission rates are considerably smaller than the modelled ones, especially in the time interval 250-500ms, thus indicating the existence of additional losses of α-particles and/or of enhanced slowing down rates. Since in the case of sawtooth activity already the source term was effected, Fig.21 illustrates only weak discrepancy between measured and modelled rates, which obviously also occurred due to faster slowing down (τ_s = 0.27s) here. For all discharges listed in Table 1, Fig.22 compares the measurements of γ-emission delay times with modelling results. Evidently, in view the large error bars, a better time resolution of γ-measurements would be desirable. If, however, such improved γ-diagnostics will confirm this pronounced difference (20-75%) between modelled and measured values shown in Fig.22, this discrepancy may be used for assessing additional transport mechanisms and evaluating alpha confinement as well as slowing down. We inject to note that the 3D Fokker-Planck simulation of fusion alphas performed here is in excellent agreement with calculations based on the CRONOS/SPOT code [9], which is illustrated for Pulse No: 61341 in Fig.23.

3.2 TEMPORAL EVOLUTION OF G-EMISSION INDUCED BY RF-HEATED ^{4}HE IONS

Time-resolved measurements of γ-ray emission induced by ICRH accelerated ^{4}He ions were carried in the a-particle simulation experiments on JET (with third harmonic ion-cyclotron-resonance heating of 116keV ^{4}He beams in ^{4}He plasmas [3, 4]). In these experiments the ICRH notches (prompt drops of the ICRH power from ≈ 8MW to ≈ (5÷6)MW for a time $0 < t < 1$s, see Fig.24) resulted in the relaxation of the maximum γ-emission rate R_{gmax}, established before the notch ($t < 0$), to a reduced level ~ $(0.4÷0.5)R_{\gamma max}$ during the notch. For the measurements a vertical gamma-detector (see Fig. 12b) with rather short integration time Δt_{int} = 100ms was used. Fig. 24 demonstrates typical time variations of P_{ICRH}, P_{NBI}, as well as of electron temperature and density in APSE. It is seen that a 40% drop of P_{ICRH} (from 7.5MW to 4.8MW) for $0 < t < 1$s in Pulse No: 63073 resulted only in a weak (≈ 0%) decrease of electron temperature and in an even smaller alteration of the electron density in the plasma centre. Correspondingly, the Spitzer slowing down time in the plasma core was reduced from $<\tau_{se}>$ ($t < 0$) ≈ 0.41s to $<\tau_{se}>$ ($t = 0.5$s) ≈ 0.34s. Simultaneously, the 40% drop of P_{ICRH} resulted in about 50% decrease in the γ-emission rate indicating a significant reduction of the population of ^{4}He ions that is accelerated above 1.6MeV. Important here is the following observation: the characteristic scale for changing the Spitzer slowing down time due to the ICRH notch is ≈ 3s and hence significantly exceeds $<\tau_{se}>$ that is smaller than the 1s notch duration. On the other hand, the characteristic time scale of R_γ-alteration due to relaxation of the ^{4}He ion distribution is small (< 0.5s) and comparable with $<\tau_{se}>$, which accords to the qualitative analysis of Sec.2.4. This circumstance allows to separate the R_γ-variations that are triggered by the relaxation of fast ^{4}He ions from those relating to the slowly varying level of the γ-emission rate during the P_{ICRH} notch, R_γ^{notch}, which is found after relaxation and evolves only due to the changing slowing time $<\tau_{se}>(t)$. Note the analogy of R_γ^{notch} with the population of fast ^{4}He ions $N_{\alpha min}$ considered in Sec. 2*d*, which was established at reduced power after relaxation of the fast ^{4}He population. The possibility of subtracting R_γ^{notch} from the total gamma emission rate is demonstrated in Fig. 25 where two JET discharges with different NBI powers but with similar PICRH reduction (≈ 40%) and similar $<\tau_{se}>$ ($t < 0$) ≈ 0.39s are compared. The dashed lines in this figure represent the fit of experimental data of R_g and the dotted marked lines demonstrate the slow time variation of R_γ induced by the change of the Spitzer slowing-down time, thus characterizing the level of gamma emission at reduced ICRH power, R_γ^{notch}. We note that the injection power of 116keV ^{4}He neutrals was kept at a steady level of 2MW (1.3MW on-axis and 0.7MW off-axis beams) for Pulse No: 3073 and at 1.35MW (on-axis beam only) for Pulse No: 63062. Although the presence of additional off-axis beam does not essentially affect the localization of energetic ^{4}He ions in the plasma as evident from Fig.26, it can essentially diminish the efficiency of ICRH heating of helium ions. The indication of a higher "effective temperature" of ICRH accelerated ^{4}He ions in the case of low P_{NBI} can be concluded from Fig.25 where for Pulse No: 63062 $R_\gamma(t)$ is seen to decay with a characteristic time much larger than the corresponding decay time in Pulse No: 63073 with higher NBI power. This effect of P_{NBI} on the effective temperature of accelerated ^{4}He ions is in agreement with classical expectations.

According to Stix formula [14] the tail temperature of ICRH accelerated ions is

$$T_{\perp} \sim P_{ICRH}\,\tau_{se} / (2n_{min}) \sim P_{ICRH} / P_{NBI} \qquad (21)$$

where $n_{\min}$ is the minority ions density. Note that this formula also yields a higher heating level of accelerated ions at reduced P_{NBI}. We point out that the dissimilarity in γ-emission relaxation†for different NBI powers is in agreement with our analytical evaluations in Sec. 2*d* as well and corresponds with the relaxation of the populations of E>1.6MeV Maxwellian alphas at different temperatures. A quantitative accurate modelling of the temporal evolution of γ-emission in APSE should be obviously based on a 3D time-dependent kinetic model of ICRH accelerated ions (accounting for collision induced diffusive and convective transport) which, however, is beyond the scope of this paper.

SUMMARY

Examination of the temporal evolution of γ-emission induced by fast alphas colliding with beryllium impurity ions in several JET discharges demonstrates the perspectives of studying fast ion behaviour using g-diagnostics. Particularly, in the case of TTE-like short term DT fusion sources leading to a fast alpha distribution far from equilibrium, the possible evaluation of particle and energy loss rates of fast alphas via the delay time between alpha induced g-emission and the fusion source is shown to be a viable technique. On the other hand, fast ions with quasi-equilibrium distributions, e.g. obtained by RF heating over a sufficiently long period, can be scrutinized by investigating the relaxation of fast ion induced γ-emission.

Our 3D Fokker-Planck modelling of γ-emission in TTE plasmas, which takes into account only first orbit loss of alphas, overestimates the measured gamma delay time thus indicating that additional losses of a-particles or enhanced energy losses of alphas may exist. Thus a considerable disagreement between modelled and measured gamma delay times was detected in current hole and low current plasmas and in those with sawtooth activity. In the case of reliable gamma diagnostics this discrepancy can be evaluated to give information on alpha confinement and slowing down. We note that in [9] modelling of gamma emission rates induced by energetic ($E > 5MeV$) minority protons during RF heating in JET demonstrated the necessity to embed some additional radial diffusion in order to reduce the difference in the temporal evolution of measured and modelled γ-emission.

In conclusion we point out that, in tritium NBI blip experiments on JET, the relatively low accuracy of delay times determined from measurements was caused mainly by the large integration time of γ-signals, which was performed for the first time [1]. For reliable verification of gamma delay times the upper limit for the time resolution of measurements should be around $0.1\tau_{s0}$ demanding, however, for a substantial increase of the alpha source power in order to attain an equivalent number of detected gammas. This can guarantee an acceptable accuracy of alpha confinement evaluation via γ-emission diagnostics in TTE-like plasmas.

The present analysis of γ-emission induced by ICRH accelerated ^{4}He-ions in alpha-particle simulation experiments in JET has confirmed the perspective of γ-diagnostics of RF heated ions in tokamaks; e.g. the experimental inspection of the relaxation of γ-emission induced by energetic RF accelerated ions can serve for evaluating their energy distribution.

Evidently, applying multi-channel measurements of the temporal evolution of g-emission induced by fast ions in tokamak plasmas should allow for investigation of spatial profiles of slowing down and loss rates of fast ions.

Finally we note, that – due to relatively low slowing down rates of fast ions in ITER ($\tau_{sa0} = \tau_{sd0}/2$~0.7-0.9s) – gamma diagnostics of time-dependent fast ion distributions look promising also of NBI deuterons (E_0 = 1MeV) in future tokamaks via nuclear reactions of D-ions with Be and/or C impurities (energy threshold 0.4MeV and 0.6MeV, respectively).

ACKNOWLEDGEMENT

This work, supported by the European Communities under the contract of Associations between EURATOM and OEAW, UKAEA and CEA, was carried out within the framework of the European Fusion Development Agreement. The views and opinions expressed herein do not necessarily reflect those of the European Commission.

REFERENCES

[1]. V.G. Kiptily, *et al.*, Phys. Rev. Lett. **93**, 115001 (2004)
[2]. D. Stork, *et al.*, Nucl. Fusion, **45**, S181 (2005)
[3]. M. Mantsinen *et al*., Phys. Rev. Lett. **88,** 105002 (2002)
[4]. V.G. Kiptily, *et al.*, Nucl. Fusion, **45**, L21-L25 (2005)
[5]. V.G. Kiptily, F.E. Cecil and S.S. Medley PPCF **48**, R59-R82 (2006)
[6]. N. Hawkes, *et al.*, Phys. Rev. Lett. **87**, 115001 (2001**)**
[7]. T . Fukita, *et al.*, Phys. Rev. Lett. **87**, 245001 (2001**)**
[8]. V.A. Yavorskij, *et al.*, 20th IAEA Fusion Energy Conference, Vilamoura, 2004, paper TH/P4-4
[9]. M. Schneider, *et al.*, Phys. Plasmas Contr. Fus. **47**, 2087 (2005)
[10]. V.A. Yavorskij, *et al.*, 32nd EPS Plasma Physics Conference, Tarragona, Spain, 2005, paper O2/02
[11]. V.A. Yavorskij, *et al.*, 21st IAEA Fusion Energy Conference, Chengdu, 2006, paper TH/P6-7
[12]. I. Voitsekhovitch, *et al.*, Nucl. Fusion **47,** 599 (2007)
[13]. J.M. Adams, *et al.*, Nucl. Fusion **31**, 891 (1991)
[14]. T.H. Stix, Nucl. Fusion **15**, 737 (1975)

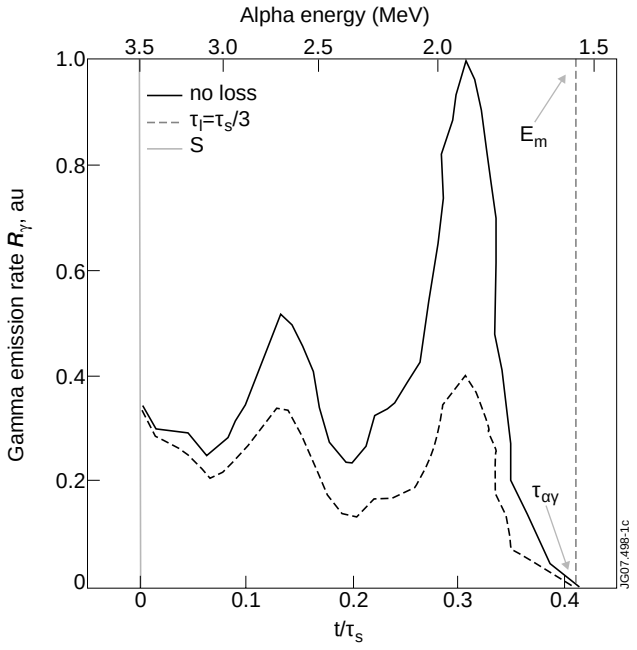

Figure 1: Evolution of gamma emission rate Rg, induced by alphas from a 3.5MeV fusion source effective only at t = 0. The solid line corresponds to perfect alpha confinement ($\tau_l >> \tau_s$) and the broken line to an alpha loss time $\tau_l = \tau_s/3$.

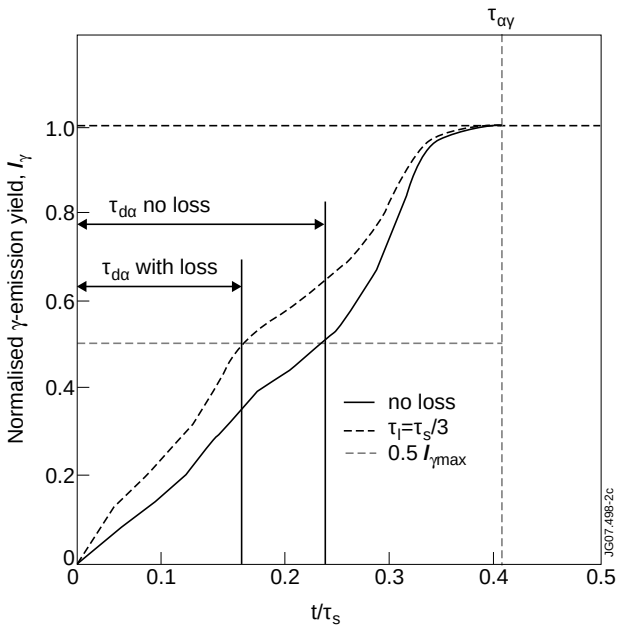

Figure 2: Evolution of normalised gamma emission yield, $I_\gamma = \int_0^t R_\gamma(t')dt' / \int_0^{t_{\alpha\gamma}} R_\gamma(t')dt'$, in the case of the same alpha source as in Fig.1. The γ-emission delay time τd_γ is defined as the time when $I_\gamma(\tau_d) = 0.5$.

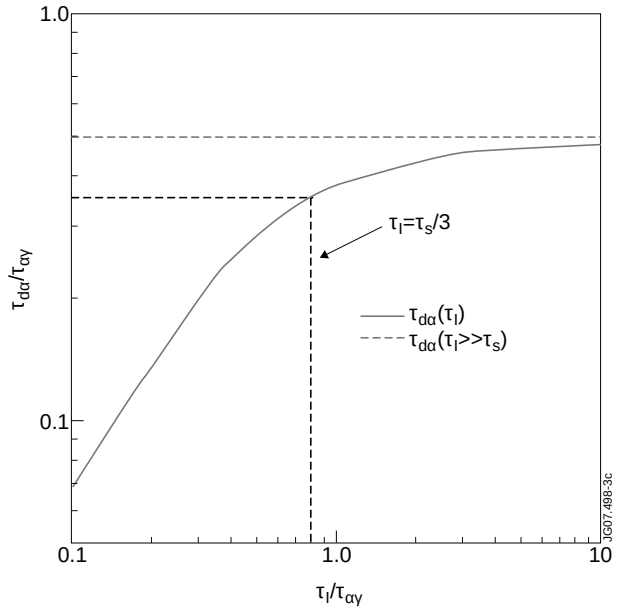

Figure 3: Delay time of the number of fast (E>1.6MeV) alphas as a function of loss time τ_l.

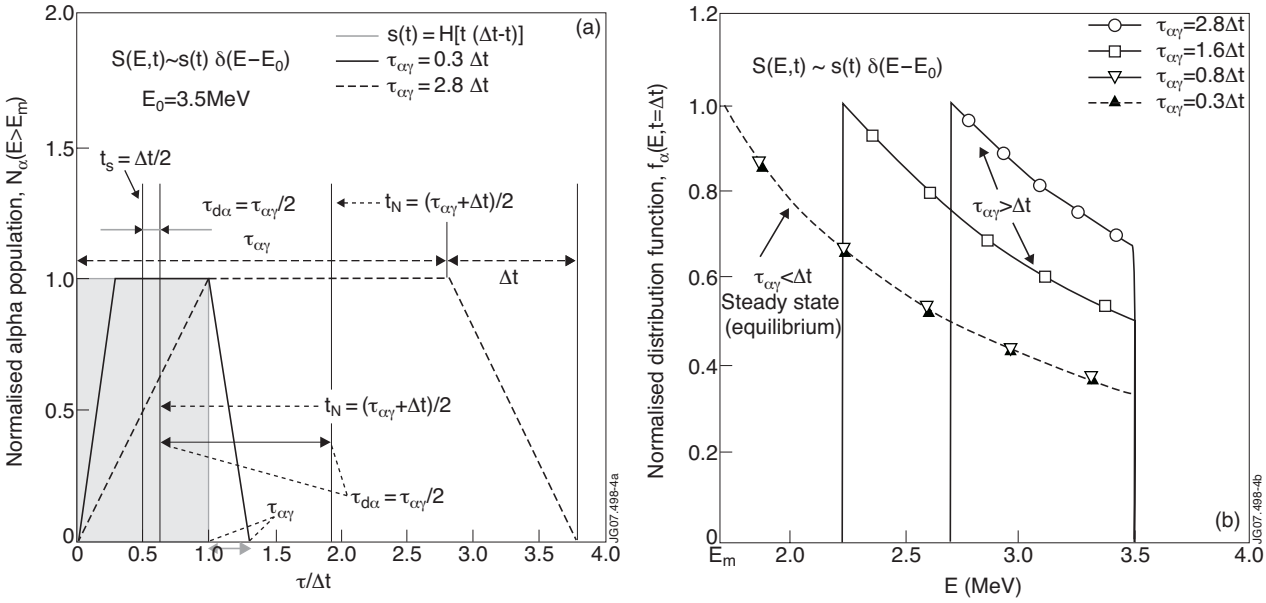

Figure 4: (a) Evolution of the density of fast alphas ($E>E_m$) produced by a monoenergetic and step-like time dependent source and (b) Energy distribution function at $t = \Delta t$ (right) depending on the ratio of $\Delta t / \tau_{\alpha\gamma}$.

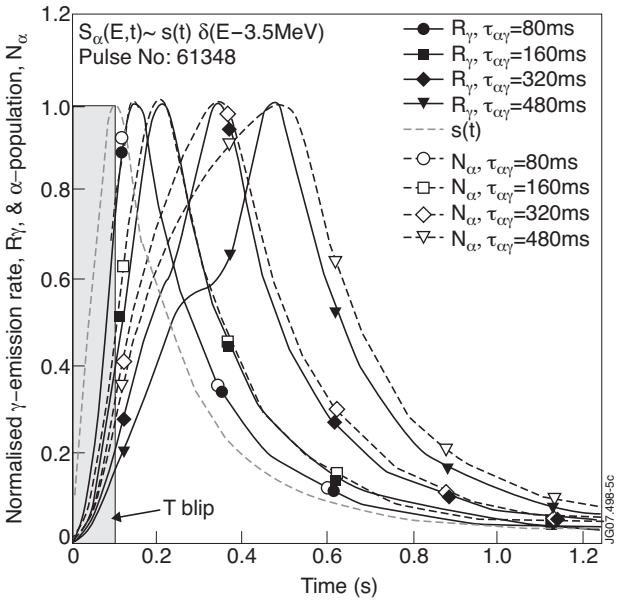

Figure 5: Evolution of gamma emission and of the density of fast (E>1.7MeV) alphas produced by mono-energetic TTE-like source (Pulse No: 61348) depending on the value of Spitzer slowing-down time (1D Fokker-Planck model).

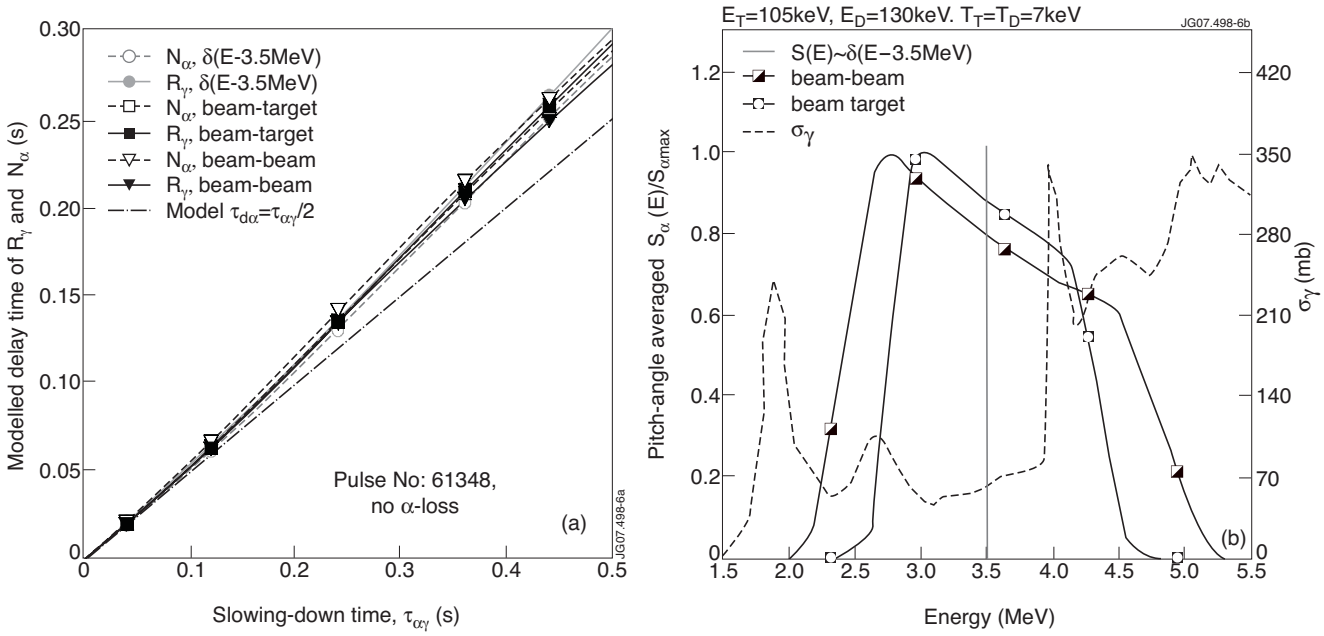

Figure 6: (a) 1D Fokker-Planck modelled delay times of gamma emission and of the density of well confined fast (E>1.7MeV) fusion alphas as a function of slowing-down time for different source energy spectra shown in (b) .

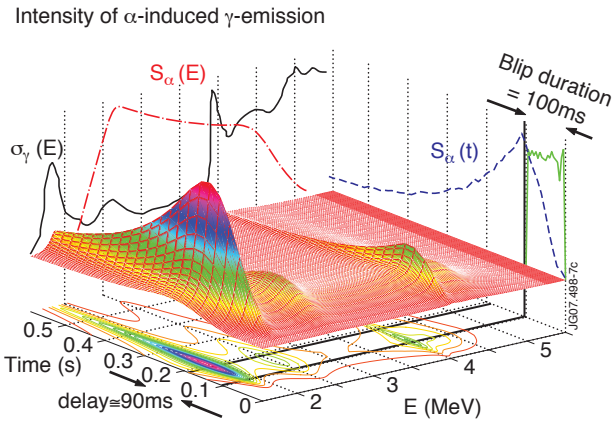

Figure 7: 3-dimensional and contour plot of the Fokker-Planck modelled intensity of alpha induced γ-emission as a function of time and alpha energy for JET Pulse No: 61346 (τ_s = 620ms, τ_{blip} = 100ms).

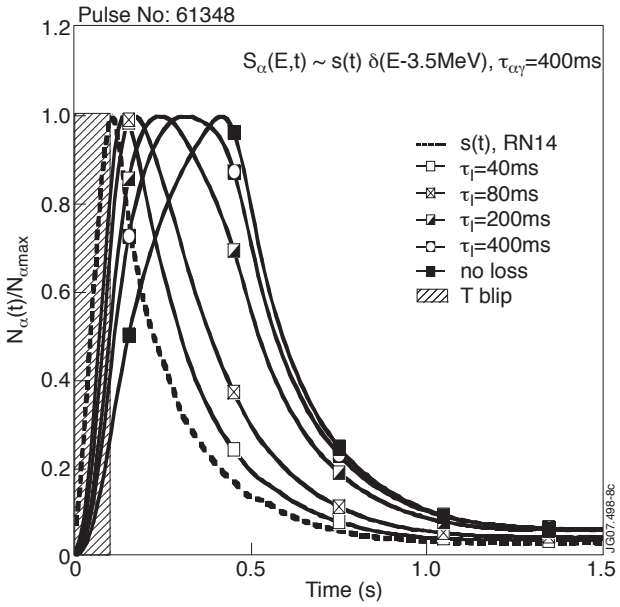

Figure 8: Evolution of the population of fast (E>E_m) alphas produced by a mono-energetic TTE-like source depending on the loss time tl for a fixed Spitzer slowing-down time τ_s =1.1s Fig. 9 Delay time of the population of fast (E> E_m) alphas as a function of loss time for two cases of Spitzer slowing-down time, τ_s =1.1s and 0.55s.

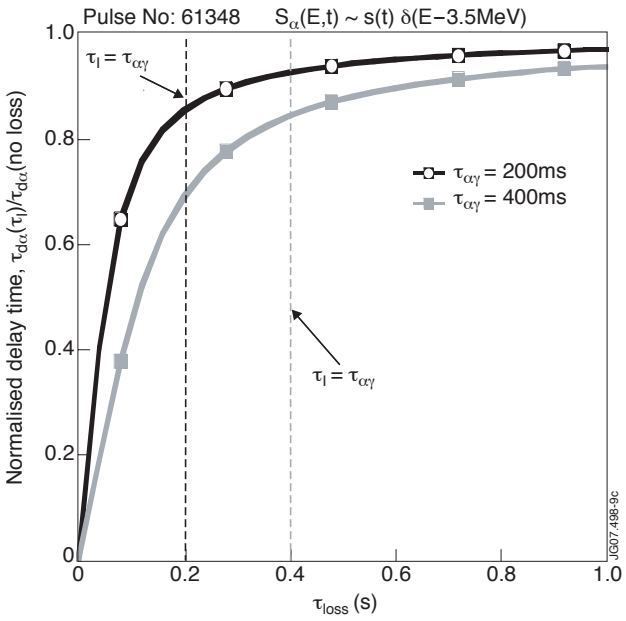

Figure 9: Delay time of the population of fast ($E>E_m$) alphas as a function of loss time for two cases of Spitzer slowing-down time, τ_s = 1.1s and 0.55s.

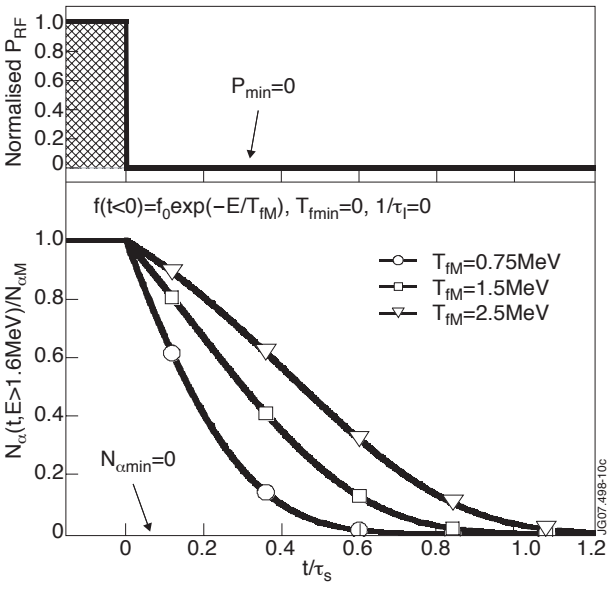

Figure 10: Full ($N_{\alpha min}/N_{\alpha min}$ = 0) relaxation of the population of fast ($E>E_m$) Maxwellian-like alphas depending on the value of the effective temperature.

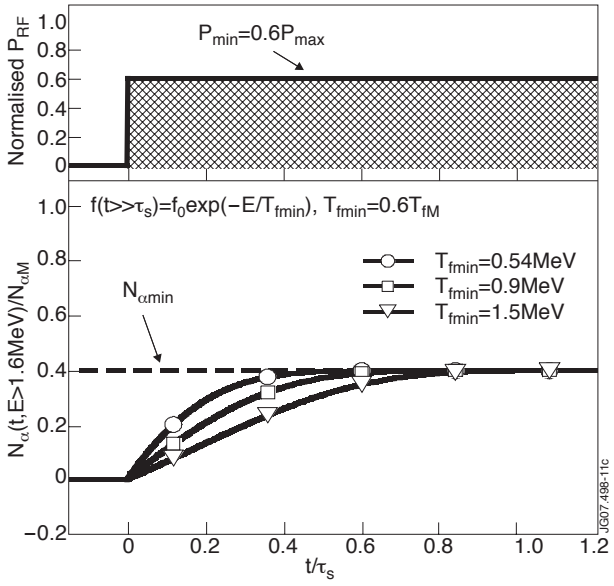

Figure 11: Evolution of the population of fast ($E> E_m$) alphas generated at t>0 by the reduced level of ICRH power depending on the value of the effective temperature.

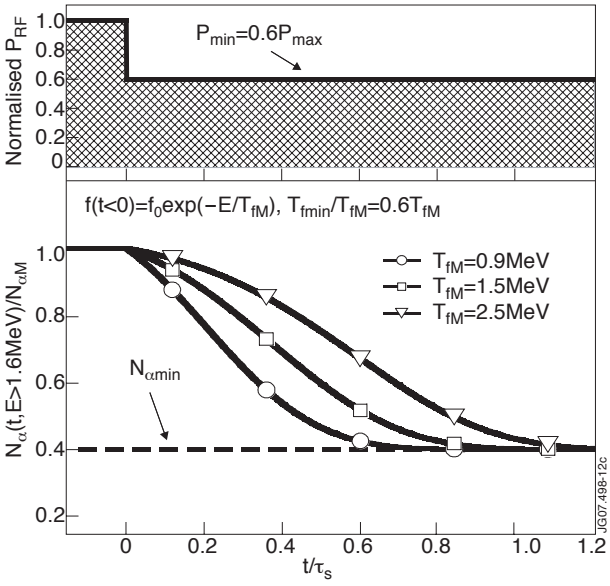

Figure 12: Partial ($N_{\alpha min}/N_{\alpha min}$=0.4) relaxation of the population of fast ($E>E_m$) Maxwellian-like alphas depending on the value of the effective temperature

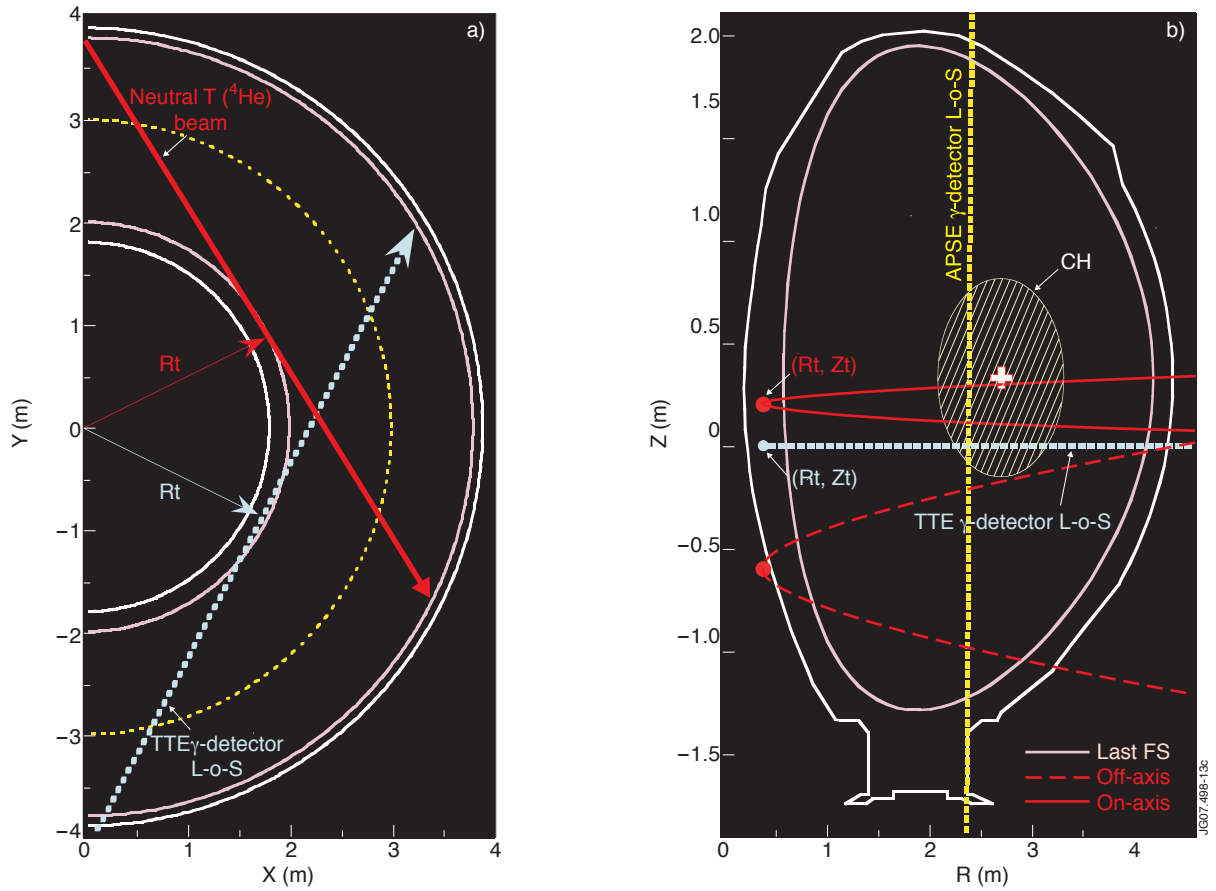

Figure 13: Gamma detectors line-of-sight (blue line – TTE, yellow line APSE) in poloidal and toroidal cross-sections in JET. Red lines show the trajectories of on-axis and off-axis tritium (^{4}He) neutral beams.

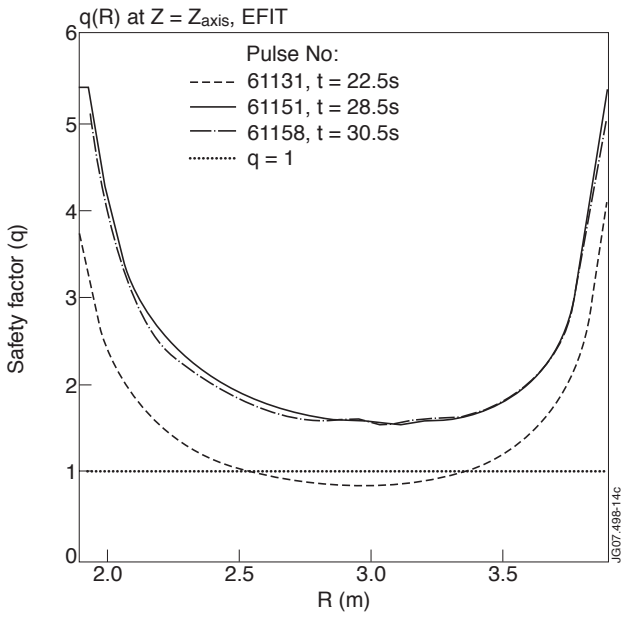

Figure 14: EFIT mead-plane q profiles at the beginning of T blip for MC Pulse No's : 61131, 61151 and 61158.

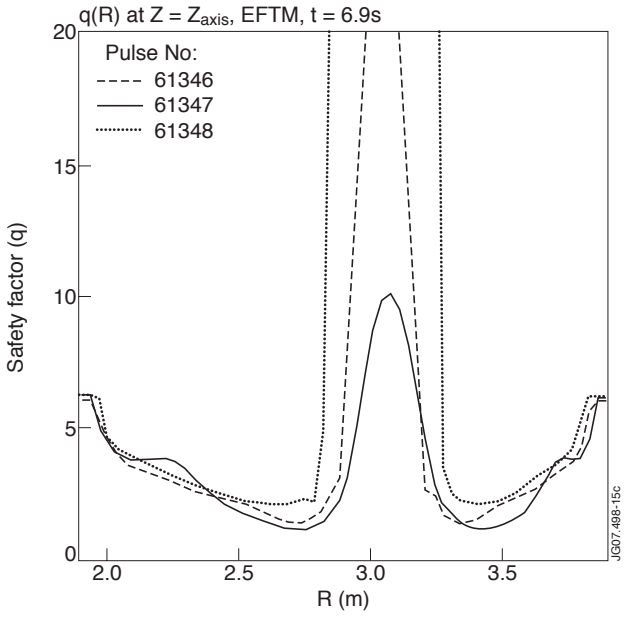

Figure 15: EFTM mead-plane q profiles in early post-blip (< 0.3s after the end of blip) CH Pulse No's: 61346, 61347 and 61348

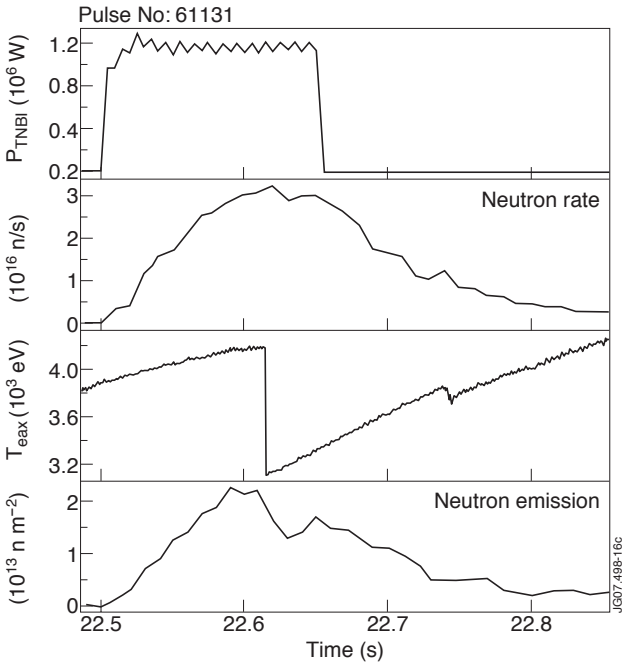

Figure 16: Sawtooth effect on electron temperature and DT fusion emissivity during tritium blip in TTE Pulse No: 61131.

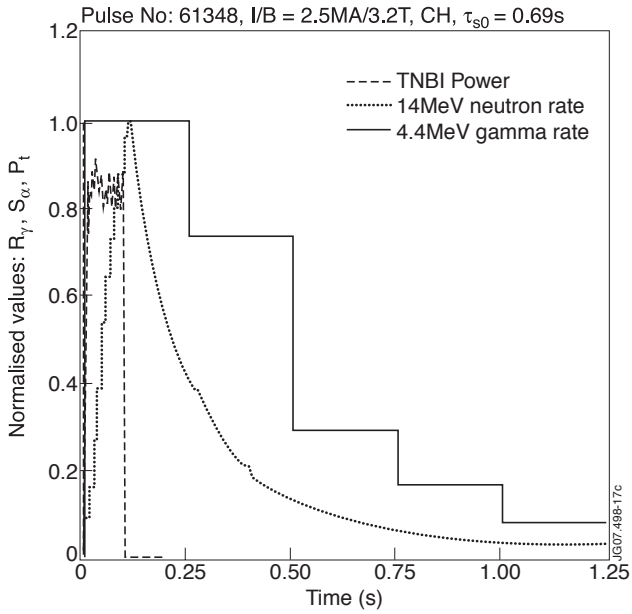

Figure17: Measured rates of gamma and neutron emission for JET Pulse No: 61348. The dashed curve represents the tritium NBI power.

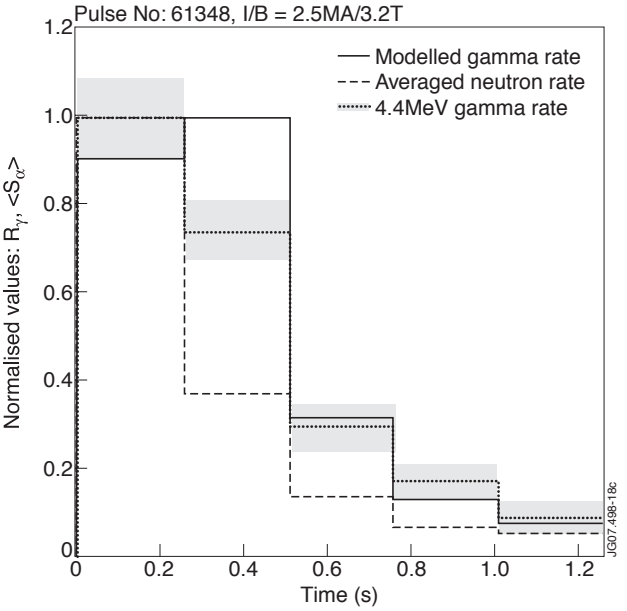

Figure 18: Measured and rates of gamma and neutron emission (averaged over 250ms integration times of γ-measurements) and modelled R_γ for JET Pulse No: 61348.

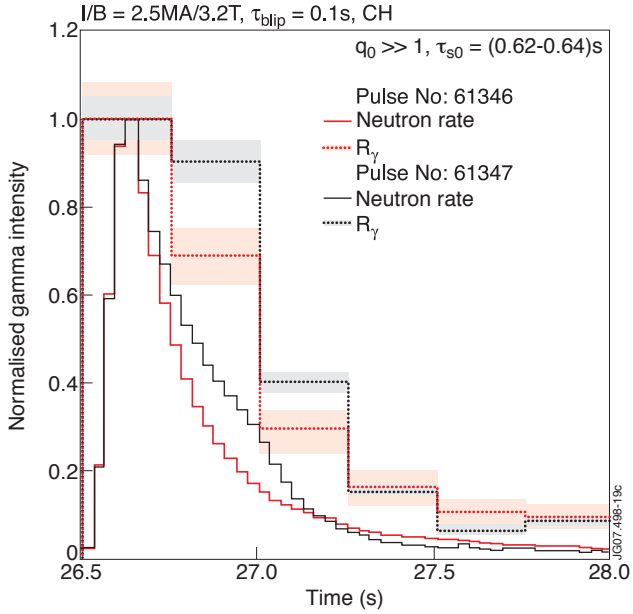

Figure 19: Measured gamma rates for Pulse No's: 61346 and 61347. In both discharges, R_γ (t) and N14(t) appear to manifest congruent discrepancies resulting in nearly equal delay times.

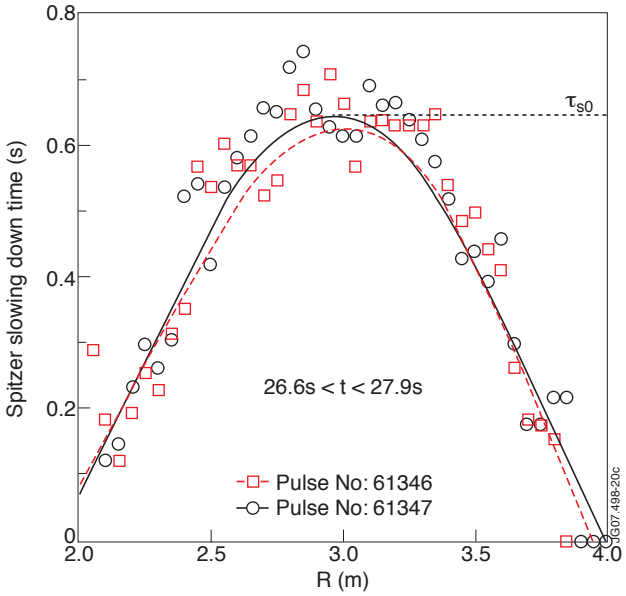

Figure 20: Experimental data and time-averaged mid-plane profiles of Spitzer times of alphas for Pulse No's: 61346(τ_{s0} = 0.62s) and 61347(τ_{s0} = 0.64s).

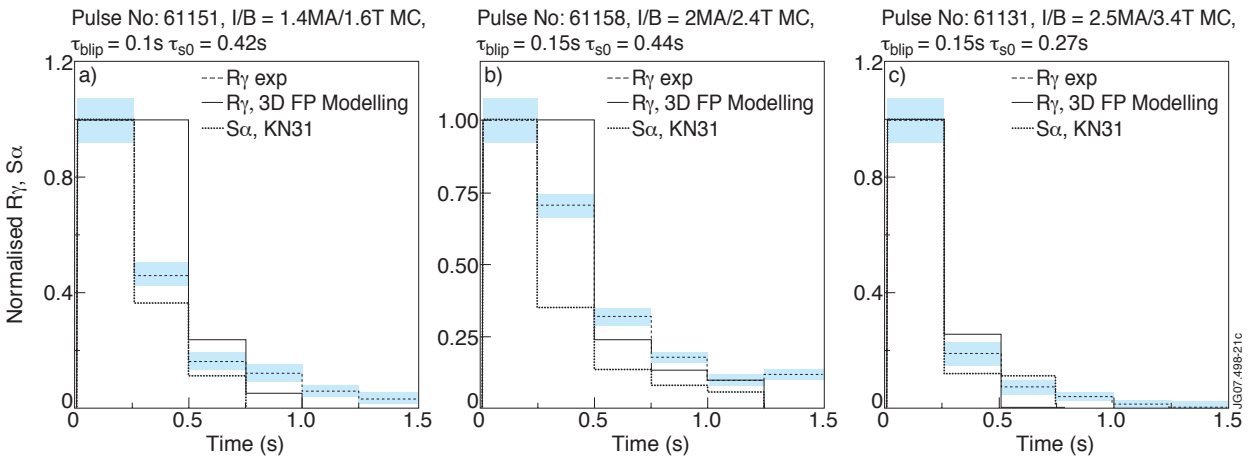

Figure 21: Measured and modelled rates of DT fusions and of gamma emission in the cases of plasmas with low current (figure a, b) and in a plasma with sawtooth activity (figure c).

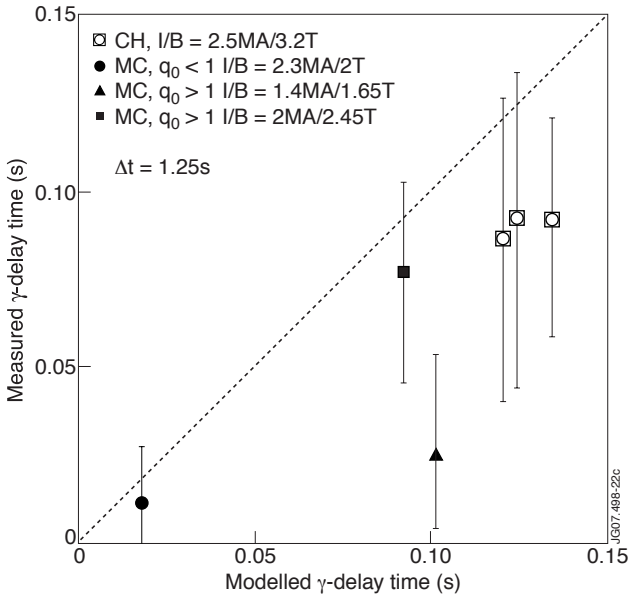

Figure 22: Measured vs modelled delay times of γ-emission based on 3D FP modelling for CH (Pulse No's: 61346 ÷ 61348) and MC (Pulse No's: 61131, 61151, 61158) plasmas in JET.

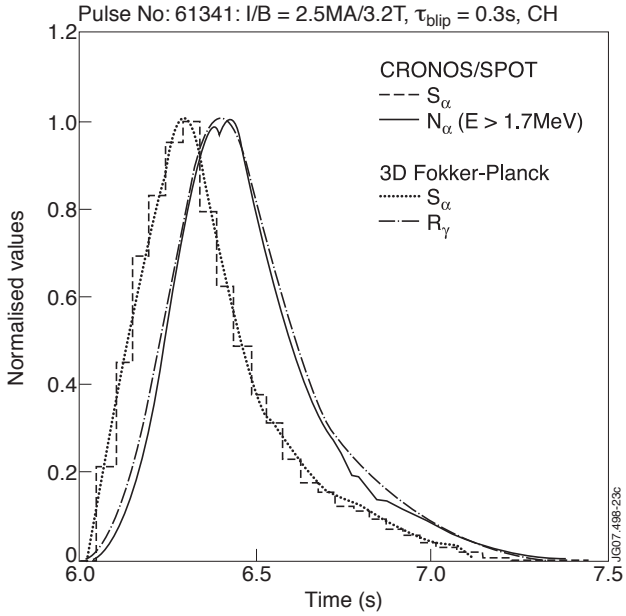

Figure 23: Comparison of Fokker-Planck modelled γ-emission rate, R_γ, and CRONOS/SPOT calculations of N_α(E>1.7MeV) for Pulse No: 61341.

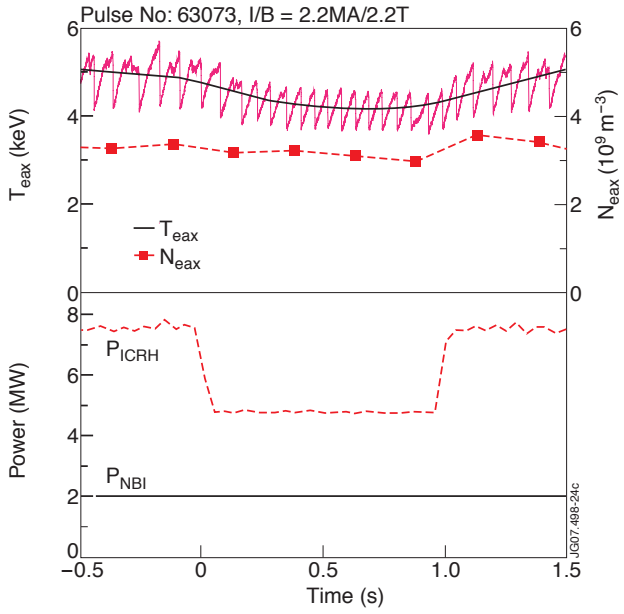

Figure 24: Time variations of ICRH and NBI power as well as of electron temperature and density at the magnetic axis in Pulse No: 63073.

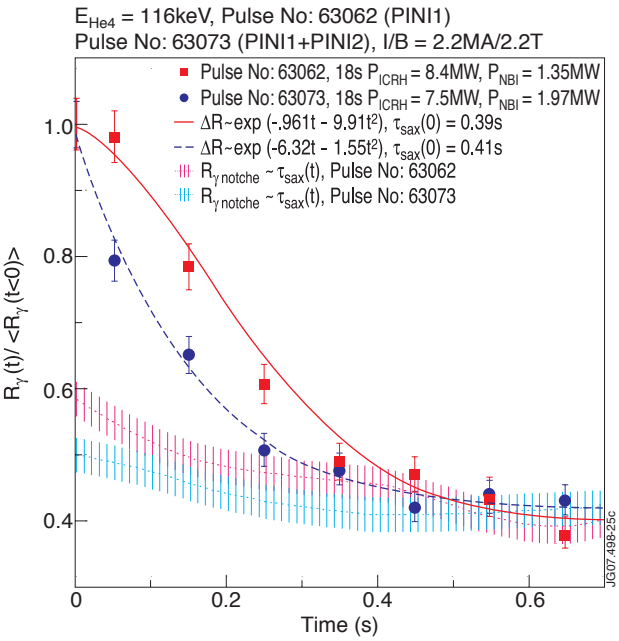

Figure 25: Relaxation of normalized γ-emission rates in Pulse No: 63073 induced by 2.7MW prompt drop of ICRH power compared to that in Pulse No: 63062 with similar 3.1MW P_{ICRH} reduction. The dotted lines represent the γ-emission level $R_\gamma^{notch} = R_\gamma(0.7s)\ \tau_{sax}(t)/\tau_{sax}(0.7s)$slowly varying according to Spitzer time changes, where τ_{sax} denotes the Spitzer slowing down time at the axis.

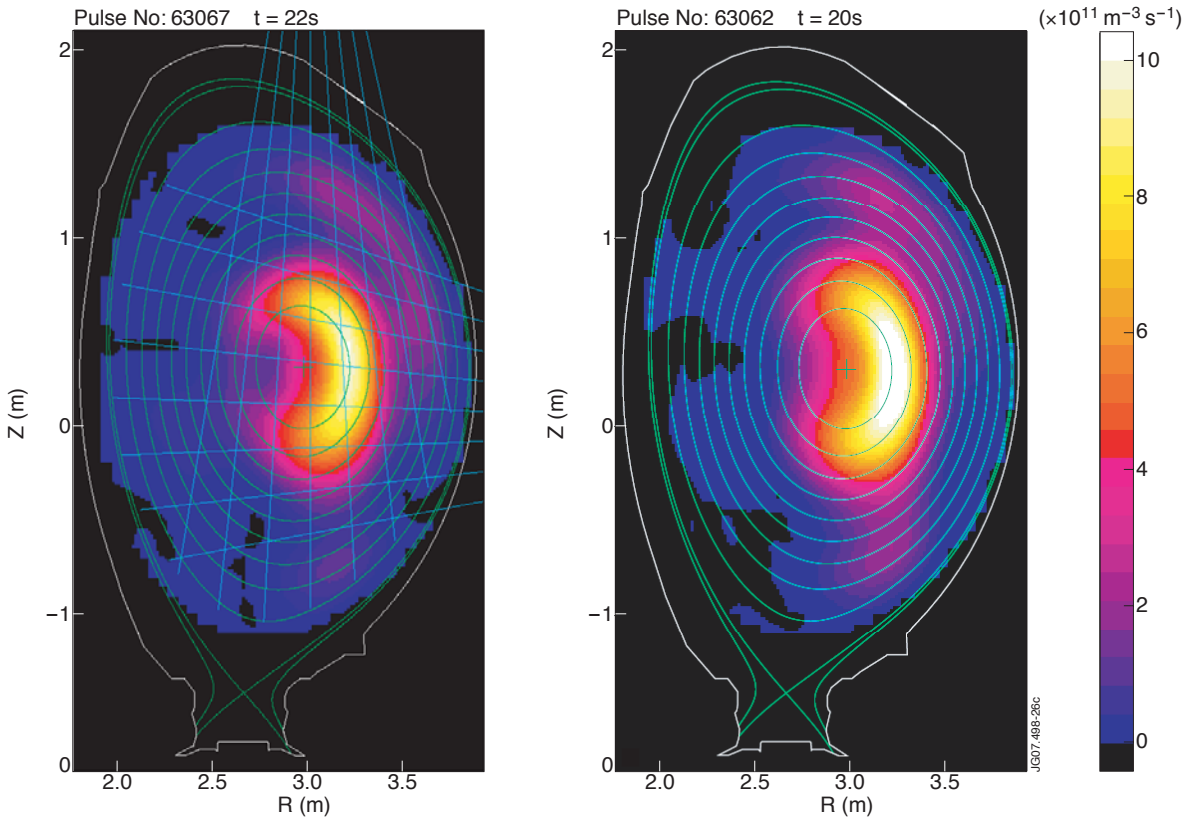

Figure 26: Poloidal images of time-averaged γ-ray emissions for Pulse No: 63067 (1.33MW on-axis and 0.64MW off-axis beams, 2s time average) and Pulse No: 63062 with 1.35MW on-axis beam only (averaged over 1s).